IPPI

Polyolefins Journal, Vol. 2 No. 2 (2015) 121-133

ORIGINAL PAPER

Mathematical modeling of the effect of catalyst initial shape and the crack pattern in olefin copolymerization

Marzieh Nouri[1], Mahmoud Parvazinia[1*], Hassan Arabi[1], Mohsen Najafi[2]

[1] Iran Polymer and Petrochemical Institute, P.O. Box 14975/112, Tehran, Iran

[2]Qom University of Technology, P. O. Box 1519-37195, Qom, Iran

Received: 14 March 2015, Accepted: 12 May 2015

ABSTRACT

A two-dimensional (2D) single particle model for the copolymerization of propylene-ethylene with heterogeneous Ziegler-Natta catalyst is developed. The model accounts for the effects of the initial shape of the catalyst and carck/ pore patterns on the copolymer composition, polymerization rate and average molecular weight properties. The spherical and oblate ellipsoidal shapes of catalyst particle and four different pattern distributions of cracks and pores in a growing particle are studied in this simulation. It is assumed that the diffusion coefficient of monomers in the cracks/pores is 10 times higher than that in the compact zone of the particle. In other word, the cracks are distinguished from the parts with higher monomer diffusion coefficient. The dynamic 2D monomer diffusion-reaction equation is solved together with a two-site catalyst kinetic mechanism using the finite element method. The simulation results indicate that the initial shape of catalyst changes the average copolymer composition only in the early stage of polymerization, but the crack/pore patterns in the growing particle have a strong impact on the copolymer composition in the polymer particles due to the change of mass transfer limitations. **Polyolefins J (2015) 2: 121-133**

Keywords: Single particle; Modelling; Finite Element Method; Polyolefin; Copolymerization

INTRODUCTION

One of the most important methods in the production of polyolefin resins (i.e. polyethylene, polypropylene and their copolymer with α-olefins) is olefin polymerization over a solid heterogeneous catalyst. The most popular catalysts in polyolefin industry are single site silica supported metallocene catalysts and multiple site Ziegler-Natta (Z-N) and chromium oxide catalysts. Polymerization reactions occur via a coordination insertion mechanism on the active sites following the diffusion of monomers either through open pores (if exists) or through the amorphous part of produced polymer. When monomer reaction occurs, one more building block of a polymer chain forms and as the polymerization proceeds the small catalyst particles with 20-100 μm in diameter grow to form a pseudo-homogeneous polymer particle with about 500-5000 μm in diameter.

The modeling of a growing catalyst-polymer particle

* Corresponding Author - E-mail: M.Parvazinia@ippi.ac.ir

in heterogeneous catalyst polymerization has been studied extensively in the open literature [1-3]. The two popular models most widely used in single particle modeling, are the polymeric flow model (PFM) [4-6] and the multigrain model (MGM) [7-8]. The PFM, first proposed by Schmeal and Street [4], assumes that the growing catalyst-polymer particle forms a continuum. It also assumes that the mass transfer in particle follows a Fickian diffusion mechanism through the pseudo-homogeneous polymer phase and catalyst sites move outwards as the particle expands due to polymerization. This pseudo-homogeneous approximation makes PFM an appropriate choice for several modeling applications [1]. Nagel et al. [7] proposed an early version of the MGM, which the polymeric particle (called macroparticle as well) is formed by an agglomerate of several much smaller microparticles and active sites fix in the center of microparticles. Two levels of mass and heat transfer resistances were considered in MGM. Both the PFM and MGM models are considered to have reasonable approximations of the actual physical and chemical phenomena taking place in a polymer particle and can estimate the overall particle polymerization rate, particle temperature and molecular properties of the produced polymer. The MGM gives a more detailed description of phenomena taking place during polymerization with Z-N catalysts, but the computational times required to obtain the polymer properties like molecular weight distribution (PDI) are extremely high and limit the use of this model in simulation studies [1].

Galvan and Tirrell [9] extended the PFM model to the case of copolymerization and Hutchinson et al. [10] modified their earlier version of MGM to include the copolymerization modeling. Their assumptions simplified the MGM and transformed that model into a modified PFM and used this model to describe the quasi-steady state copolymerization of the single site heterogeneous catalyst. Debling and Ray [11] classified the copolymer morphology systems into two groups: homogeneous morphology systems which describe the homopolymer, random copolymer and terpolymer products produced in single stage processes and heterophasic morphology systems which are considered when the polymer particle consists of distinct polymeric phases coexisting in the particle like the impact polypropylene produced in multi stage processes. They declared that in impact polypropylene particle, ethylene-propylene rubber flows out of the microparticle and the particle changes from a multigrain to a polymeric flow morphology. Hoel et al. [12] used PFM to model ethylene-propylene copolymerization with a metallocene single site catalyst in slurry polymerization. They modeled only comonomer composition distribution (CCD) and did not consider the PDI. It was concluded that the mass transfer limitations were responsible for broad CCD. These results were limited to amorphous polymer particle by authors.

Several varieties of multigrain and polymeric flow models have also been considered. There are the extended versions of MGM, like polymeric multigrain model (PMGM) [13-14] which neglects the diffusion resistance at the microparticle level and polymeric multilayer model (PMLM) [15-16] which ignores the microparticle in order to improve the initial MGM model.

Najafi et al. [17] introduced a two-dimensional polymeric flow model to consider the fragment pattern effects on the average molecular weight properties, polymerization rate and particle overheating in heterogeneous Ziegler-Natta olefin homopolymerization. In this article, the two-dimensional polymeric flow model has been extended to model the particle growth and spatial monomer profiles in a copolymerization reaction. The model accounts for the effects of the initial shape of the catalyst and carck/pore patterns on the copolymer composition, polymerization rate and average molecular weight properties. A two-site copolymerization kinetic scheme has been used to describe propylene-ethylene random copolymerization over a heterogeneous Z-N catalyst.

Model Development

Kinetic Mechanism

A kinetic model based on two catalytic lumped sites is used to predict the monomers consumption rates and molecular weight averages (M_n and M_w) based on the method of moments in a heterogeneous multi-site Z-N catalyst. When the method of moments is used, generally two site types are enough to obtain a reasonable M_n and M_w [18]. Each lumped site is assumed to be activated instantaneously. Despite the catalyst being used, the most generally accepted mechanism for the olefin copolymerization reaction is

based on the terminal group model [19]. In the terminal group model, the polymerization kinetic constants depend on the type of monomer participating in the reaction and the type of monomer at the end of the polymer chain. In this study, the terminal model kinetic mechanism including chain initiation, propagation, site transformation and deactivation was considered (Table 1). $P_{n,i}^k$ and $D_{n,i}^k$ denote the concentrations of living and dead copolymer chains of total length n, with monomer i at the end of chain on the kth type of active site, respectively. C^{*k} and C_d^k respectively are the concentration of active and deactive of the kth type of catalyst sites. For the present simulation, propylene is monomer type A and ethylene is monomer type B.

The definition of typical variables in copolymerization reaction comes as follow:

$$F_A^k = \frac{\sum_{\mathrm{n}} F_{n,A}^k}{\sum_{\mathrm{n}} \left(F_{n,A}^k + F_{n,B}^k\right)}; F_B^k = 1 - F_A^k \tag{1}$$

Table 1. Simple kinetic mechanism for catalytic copolymerization.

Description	Reaction	Kinetic Constant
Initiation	$C^{*k} + A \rightarrow P_{1,A}^k$	K_{iA}^k
	$C^{*k} + B \rightarrow P_{1,B}^k$	K_{iB}^k
Propagation	$P_{n,A}^k + A \rightarrow P_{n+1,A}^k$	K_{pAA}^k
	$P_{n,A}^k + B \rightarrow P_{n+1,B}^k$	K_{pAB}^k
	$P_{n,B}^k + A \rightarrow P_{n+1,A}^k$	K_{pBA}^k
	$P_{n,B}^k + B \rightarrow P_{n+1,B}^k$	K_{pBB}^k
Transfer	$P_{n,A}^k \rightarrow C^{*k} + D_{n,A}^k$	K_{trA}^k †
	$P_{n,A}^k + H \rightarrow C^{*k} + D_{n,A}^k$	
	$P_{n,B}^k \rightarrow C^{*k} + D_{n,B}^k$	K_{trB}^k †
	$P_{n,B}^k + H \rightarrow C^{*k} + D_{n,B}^k$	
Deactivation	$P_{n,A}^k \rightarrow C_d^k + D_{n,A}^k$	K_{dac}^k
	$P_{n,B}^k \rightarrow C_d^k + D_{n,B}^k$	
	$C^{*k} \rightarrow C_d^k$	

† $\overline{K}_{tr}^k = K_{t\beta}^k + K_{tH}^k[H_2]$

$$f_A = \frac{A}{A+B}; f_B = 1 - f_A \tag{2}$$

$$P_n^k = P_{n,A}^k + P_{n,B}^k; D_n^k = D_{n,A}^k + D_{n,B}^k \tag{3}$$

$$M = A + B \tag{4}$$

Where F_A^k and f_A are the chains fraction formed at the kth type of active site terminated in monomer A and monomer A fraction in the particle, respectively. P_n^k and D_n^k are the concentrations of living and dead copolymer chains of the total length n on the kth type of active site, respectively, and M is the total concentrations of monomers in the particle. It should be noted that F_A^k and F_B^k do not depend on the chain length [20].

For the multi-component polymerization, the use of pseudo-kinetic rate constants (Table 2) can largely simplify the kinetic rate expressions [21]. Based on the postulated kinetic mechanism, one can define the ν^{th} living (λ) and the dead (μ) moments of the corresponding number chain length distributions at the kth type of active site:

$$\lambda_\nu^k = \sum_{n=1}^{\infty} n^\nu P_n^k \tag{5}$$

$$\mu_\nu^k = \sum_{n=2}^{\infty} n^\nu D_n^k \tag{6}$$

Accordingly, the net production/consumption rate for each monomer can be written as:

$$R_{pA} = \sum_{k=1}^{2} \left(K_{pAA}^k F_A^k + K_{pBA}^k F_B^k\right)\left[\lambda_0^k\right][A] \tag{7}$$

$$R_{pB} = \sum_{k=1}^{2} \left(K_{pBB}^k F_B^k + K_{pAB}^k F_A^k\right)\left[\lambda_0^k\right][B] \tag{8}$$

The net production/consumption rates of all other

Table 2. Pseudo-kinetic constants for binary copolymerization.

Pseudo-kinetic constant	Definition
$\overline{K}_i^k$	$K_{iA}^k F_A^k + K_{iB}^k F_B^k$
$\overline{K}_p^k$	$K_{pAA}^k F_A^k f_A + K_{pAB}^k F_A^k f_B + K_{pBA}^k F_B^k f_A + K_{pBB}^k F_B^k f_B$
$\overline{K}_{tr}^k$	$K_{trA}^k F_A^k + K_{trB}^k F_B^k$
$\overline{K}_{dac}^k$	$K_{dacA}^k F_A^k + K_{dacB}^k F_B^k$

Table 3. Net production-consumption rates of the various molecular species.

Active site	$R_{[C^{*k}]} = -(\overline{K}^k_{dac} + \overline{K}^k_i[M])[C^{*k}] + \overline{K}^k_{tr}[\lambda^k_0]$
0th Moment of living chains	$R_{[\lambda^k_0]} = \overline{K}^k_i[C^{*k}][M] - (\overline{K}^k_{tr} + \overline{K}^k_{dac})[\lambda^k_0]$
1st Moment of living chains	$R_{[\lambda^k_1]} = \overline{K}^k_i[C^{*k}][M] - (\overline{K}^k_{tr} + \overline{K}^k_{dac})[\lambda^k_1] + \overline{K}^k_p[\lambda^k_0][M]$
2ed Moment of living chains	$R_{[\lambda^k_2]} = \overline{K}^k_i[C^{*k}][M] - (\overline{K}^k_{tr} + \overline{K}^k_{dac})[\lambda^k_2] + \overline{K}^k_p([\lambda^k_0] + 2[\lambda^k_1])[M]$
0th Moment of dead chains	$R_{[\mu^k_0]} = (\overline{K}^k_{tr} + \overline{K}^k_{dac})[\lambda^k_0]$
1st Moment of dead chains	$R_{[\mu^k_1]} = (\overline{K}^k_{tr} + \overline{K}^k_{dac})[\lambda^k_1]$
2ed Moment of dead chains	$R_{[\mu^k_2]} = (\overline{K}^k_{tr} + \overline{K}^k_{dac})[\lambda^k_2]$

molecular species are reported in Table 3. The kinetic constants used in the model simulation are given in Table 4 (based on values previously used by Soares et al. [22]). To calculate the number and weight average chain lengths of the polymer chains produced over the two-site catalyst ($\overline{X}_n$ and $\overline{X}_w$), the following equations were used:

$$\overline{X}_n = \frac{\sum_{k=1}^{2}\left(\lambda_1^k + \mu_1^k\right)}{\sum_{k=1}^{2}\left(\lambda_0^k + \mu_0^k\right)} \quad ; \overline{X}_w = \frac{\sum_{k=1}^{2}\left(\lambda_2^k + \mu_2^k\right)}{\sum_{k=1}^{2}\left(\lambda_1^k + \mu_1^k\right)} \qquad (9)$$

In Table 5 the values of the physical and transport properties are reported.

Two-dimensional Particle Growth Model

In the present study, the monomers concentration in a growing polymer particle was calculated based on a two-dimensional (in r and θ spherical coordinates) dynamic diffusion-reaction model introduced in [17]. In this two-dimensional polymeric flow model, similar to PFM, a growing catalyst-polymer particle forms a continuum and is approximated by a pseudo-homogeneous medium. The particle is assumed isothermal in slurry and there is no external boundary transfer resistance. It is assumed that the mass transport of both monomers happenes by the diffusion only and is independent from time. The mass transfer resistance of all the other species (Table 3) is assumed to be negligible.

Based on the above assumptions, the governing 2D diffusion-reaction equation for the each monomer concentration, A or B, in a growing catalyst-polymer particle can be written as follows:

$$\frac{\partial A}{\partial t} = \frac{1}{r^2}\frac{\partial}{\partial r}\left(D_A r^2 \frac{\partial A}{\partial r}\right) + \frac{1}{r^2 \sin\theta}\frac{\partial}{\partial \theta}\left(D_A \sin\theta \frac{\partial A}{\partial \theta}\right) - R_{pA} \qquad (r,\theta) \in \Omega_t \qquad (10)$$

Boundary conditions:

Table 4. The numerical values of the kinetic rate constants [22].

Reaction constant	Site 1	Site 2	Dimension
K^k_{iA}	0.6	0.6	m³/mol.s
K^k_{iB}	2	2	m³/mol.s
K^k_{pAA}	0.2	0.4	m³/mol.s
K^k_{pAB}	2	4	m³/mol.s
K^k_{pBB}	2	4	m³/mol.s
K^k_{pBA}	0.2	0.4	m³/mol.s
K^k_{trA}	1.65	1.65	1/s
K^k_{trB}	1.65	1.65	1/s
K^k_{dacA}	$2x10^{-4}$	$2x10^{-4}$	1/s
K^k_{dacB}	$2x10^{-4}$	$2x10^{-4}$	1/s

Table 5. Physical and transport properties.

Description		Value	Kinetic Constant
D_A D_B	Effective monomer diffusion coefficient	$3.6x10^{-10}$ $5.13x10^{-10}$	m²/s
A_b B_b	Bulk monomer concentration	1600 400	mol/m³
M_{mA} M_{mB}	Molecular weight of monomer	$4.2x10^{-4}$ $2.8x10^{-4}$	Kg/mol
c_0^{*k}	Initial concentration of active site (k=1 and 2)	$2.5x10^{-2}$	mol/Kg_{cat}
ρ_c	Catalyst density	2840	Kg/m³
ρ_p	Copolymer density	900	Kg/m³
R_0	Initial radius of catalyst	$2x10^{-5}$	m

$$A(r,\theta,t) = A_b \qquad (r,\theta) \in \Gamma_t \tag{11}$$

$$\frac{\partial A}{\partial \theta} = 0 \qquad \theta = 0 \ \& \ \theta = \pi \tag{12}$$

$$\frac{\partial A}{\partial r} = 0 \qquad r = 0 \tag{13}$$

Initial condition:

$$A(r,\theta,0) = 0 \qquad (r,\theta) \in \Omega_0 \tag{14}$$

Where D_A is the diffusion coefficient of monomer A in a growing particle and R_{pA} (mol/m^3.s) is the polymerization rate of monomer A. Ω_t and Γ_t are the internal and boundary particle domains at time t, respectively. Ω_0 is the particle domain at time 0 and A_b is the monomer concentration at the external particle surface. Similar equations can be used for monomer B.

Two-dimensional dynamic molar conservation equation of the species ($X : C^{*k}, \lambda_\nu^k$ and μ_ν^k , ν =0, 1 and 2 and k =1and 2) in the growing particle can be derived as follows:

$$\frac{\partial X}{\partial t} = \frac{1}{r^2}\frac{\partial}{\partial r}\left(r^2 u X\right) + \frac{1}{r\sin\theta}\frac{\partial}{\partial \theta}\left(uX\sin\theta\right) + R_X \tag{15}$$

Boundary condition:

$$\int_{\Omega_t} \frac{dX}{dt} d\Omega_t = \oint_{\Gamma_t} X u d\Gamma_t \tag{16}$$

Initial condition:

$$X(r,\theta,0) = X_0 \qquad (r,\theta) \in \Omega_0 \tag{17}$$

Where R_x is the production-consumption rate of species X (see Table 3). At time zero, the concentrations of $\lambda_{\nu,0}^k$ and $\mu_{\nu,0}^k$ will be equal to zero while the concentration of the catalyst active sites at time t = 0, C_0^{*k}, will be equal to a selected value (see Table 5).

As the polymerization proceeds the small catalyst grows with time. Assuming that the polymer phase behaves as an incompressible medium, the following pseudo-steady state two-dimensional mass conservation equation can be used to calculate the copolymer particle volume:

$$\frac{1}{r^2}\frac{\partial}{\partial r}(r^2 u) + \frac{1}{r\sin\theta}\frac{\partial}{\partial \theta}(u\sin\theta) - \frac{R_{pA}M_{mA} + R_{pB}M_{mB}}{\rho_P} = 0 \qquad (r,\theta) \in \Omega_t \tag{18}$$

Boundary condition:

$$\int_{\Omega_t}\left(\frac{R_{pA}M_{mA} + R_{pB}M_{mB}}{\rho_P}\right) d\Omega_t = \oint_{\Gamma_t} u d\Gamma_t \tag{19}$$

where u (m^3/m^2.s) denotes the flux volumetric flow rate of the growing polymer phase.

The monomer(s) diffusion-reaction equation (Eq. (10)) is numerically solved using the Galerkin finite element scheme to evaluate the nodal value of monomer concentration. This equation after discretization establishes a system of linear algebraic equations equal to the number of nodes in the computational domain. The total mass conservation equation (Eq. (15)), is solved to calculate the flux volumetric flow rate of the growing polymer particle. This equation after discretization also establishes linear algebraic equations but equal to the number of elements in the computational domain. The molar species conservation equations (Eq. (18)) are solved to calculate the lumped values of the molar species concentration of the growing polymer particle. The solution of these equations in discrete form is the main challenge because it represents a huge system of simultaneous ordinary differential equations (ODEs). More details of the numerical method to solve moving boundary and the algorithm which is used to solve the equations are presented by Najafi et al. [23] and also the validation of the modeling results are explained before [17, 24].

RESULTS AND DISCUSSION

The proposed two-dimensional dynamic mathematical model is used to assess the effects of the initial particle shape and the different patterns of cracks and pores distribution in a particle on the polymerization rate, average molecular weight and copolymer composition in heterogeneous Z-N propylene-ethylene random copolymerization. In this work, an in-house developed MATLAB code is used. To make it possible to simulate all these cases, particularly the inclusion of cracks, the

method developed by Najafi et al. [17] is used in all simulations.

Effect of Initial Shape of Catalyst

Three different shapes of catalyst particle were studied in the simulation are shown in Figure 1. Case I is spherical catalyst and cases II and III are ellipsoidal with different geometric characteristics (r_x, r_y and r_z) that specify semi-major axis lengths. Case II is an oblate ellipsoid with $r_x/r_y/r_z$=2/2.82/2.82 and case III is an extreme case with $r_x/r_y/r_z$=1/1/8. It should be pointed out that the volume of initial catalyst for all three cases was the same and the total amount of active sites was the same as a result.

In Figure 2, the propylene and ethylene concentrations in the particle are depicted with respect to the polymerization time for a spherical catalyst. Although the concentrations of both monomers decrease toward the center of the particle due to the mass transport limitations, the ethylene monomer concentration in the large zone of the particle is low. It seems that high reaction rate of ethylene monomer despite of its higher diffusion rate leads to a lot of ethylene monomer consumption before reaching to the center zone of the particle. Therefore, the polymer chains grow in the center of the particle containing a higher percentage of the propylene monomer. This can be clearly seen in Figure 3. In the early stages of polymerization (for example 15 seconds of polymerization that depicted in Figure 3), ethylene monomer access to the center of

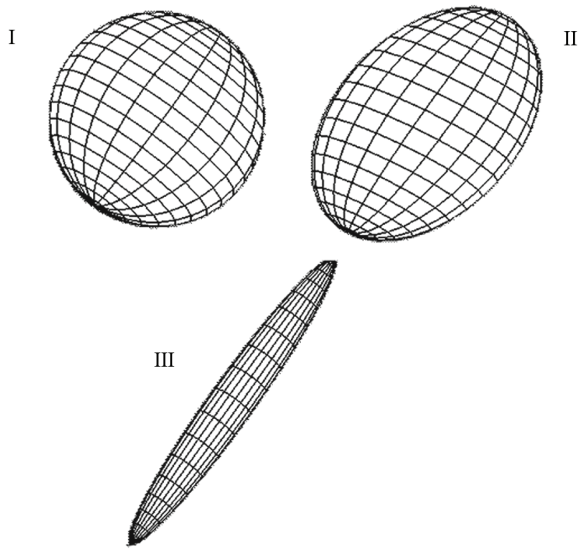

Figure 1. Different shapes of catalyst particle (cases I, II and III).

particle is easy and propylene content in a smaller zone of particle is near to maximum. When polymerization reaction progresses and the particle size increases the amount of ethylene monomer in the center of particles reduces. Generally it can be said that the distribution of propylene monomer in the polymer chains becomes broader with increasing the polymerization time.

In Figure 3 the rate of polymerization is shown as well. At the beginning of polymerization, the rate of polymerization at the center of the particle is much lower than that in the surface because of less monomers concentration. By the progress of the reaction, the reaction rate difference between the surface and the

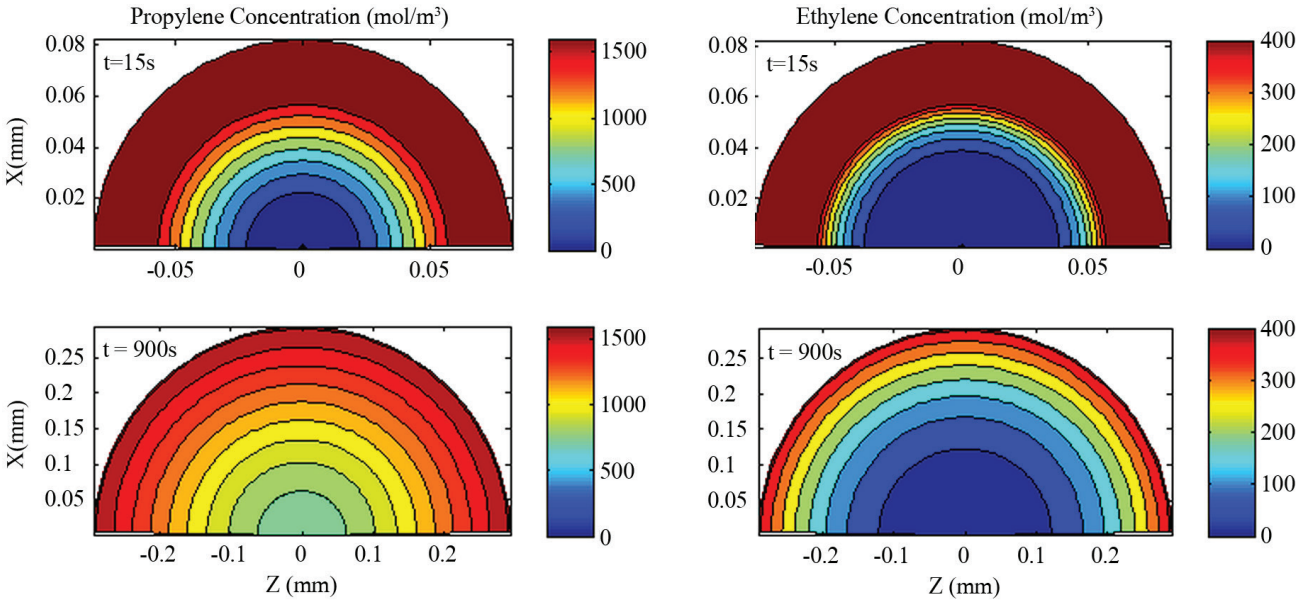

Figure 2. Contour plots of propylene and ethylene concentrations (mol/m³) in the particle in two different times (case I).

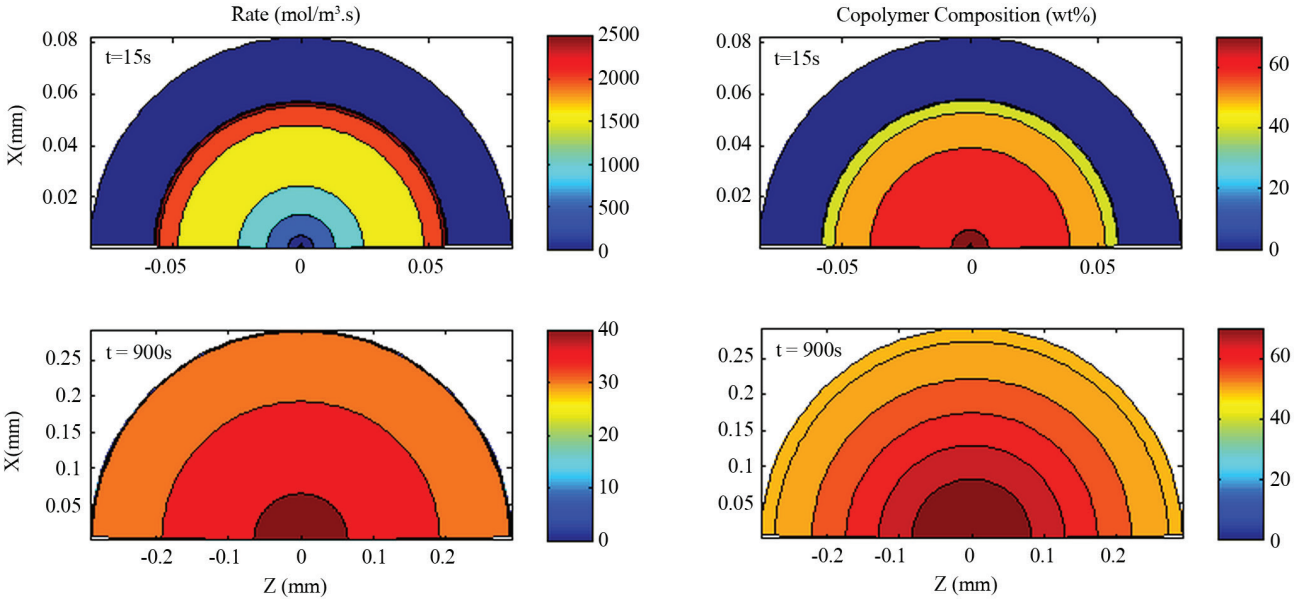

Figure 3. Contour plots of the rate of polymerization (mol/m³.s) and propylene copolymer composition (wt%) in the particle in two different times (case I).

center of the particle decreases. As the concentration of active sites is greater, the reaction rate is slightly higher in the center.

When the shape of initial catalyst is ellipsoidal, ethylene concentration is higher in more parts of the particle because the ratio of surface area to volume increases. Figure 4 shows the distribution of ethylene and propylene monomer in an oblate ellipsoid (case III) in two different times. In this case, the volume of the particle zones with higher propylene concentration will be smaller. As the particle grows, the volume of particle increases and the effect of surface area decreases as well. As can be seen in Figure 5, in the oblate ellipsoid the propylene composition weight percent in the center of the particle from 65% in 15 second has been reached to 73% in 900 second. The rate of polymerization is also affected by the large surface area to the volume ratio in ellipsoid (compare with sphere). In the first moments, the rate of polymerization in the surface is about four times

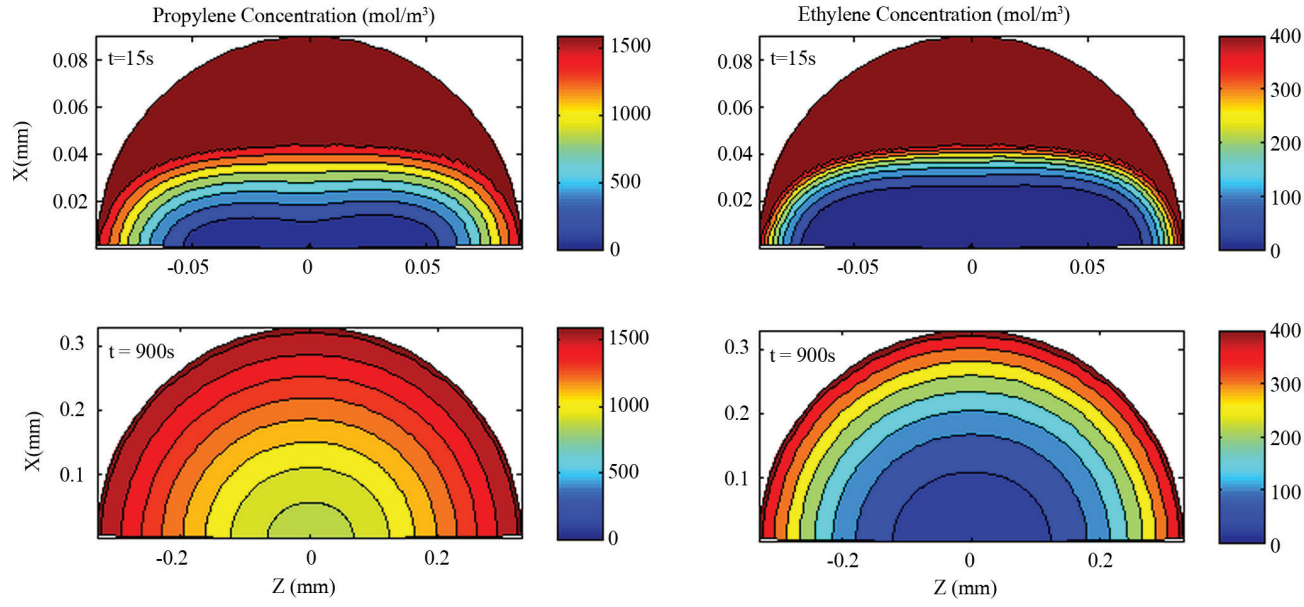

Figure 4. Contour plots of propylene and ethylene concentrations (mol/m³) in the particle in two different times (case III).

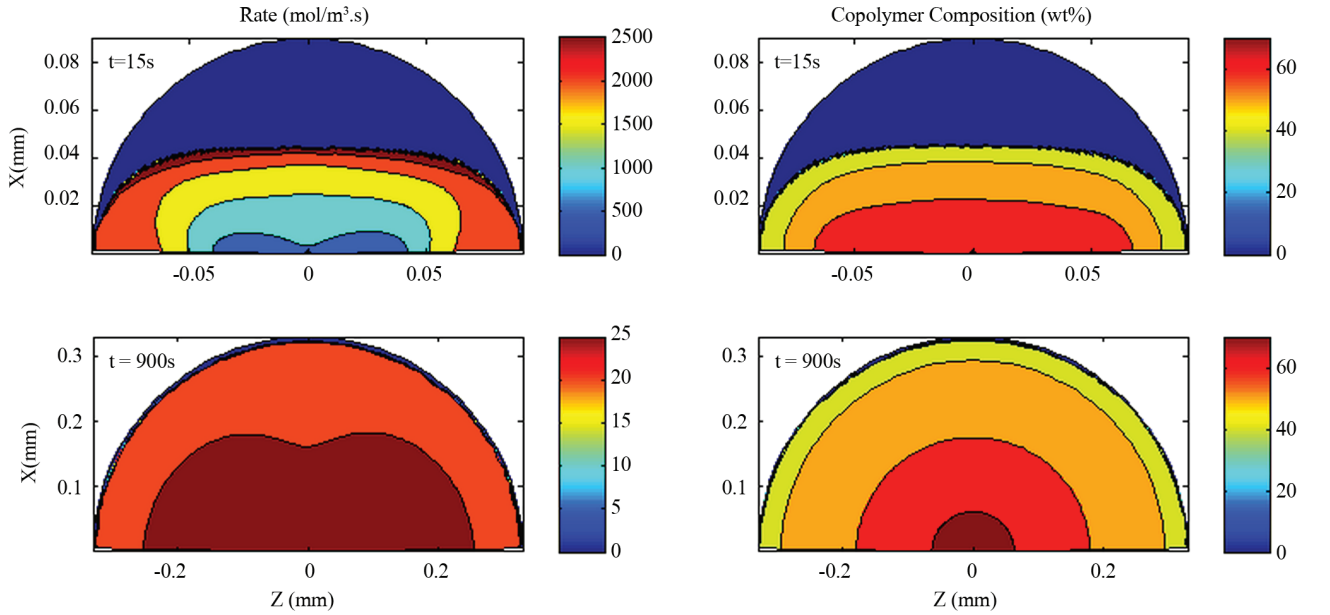

Figure 5. Contour plots of the rate of polymerization (mol/m³.s) and propylene copolymer composition (wt%) in the particle in two different times (case III).

higher than that in the center. But after a while, when the volume of the particle increased, a trend similar to sphere could be observed.

The effect of initial shape of catalyst on the number average degree of polymerization ($\bar{X}_n$) and PDI are shown in Figure 6. Although some differences can be observed in the first few seconds, after about 100 s, $\bar{X}_n$ and PDI are almost independent of the catalyst initial shape. In Figure 7, the time evolution of the overall particle polymerization rate (a) and propylene composition (wt%) (b) for different shapes of initial catalyst are illustrated. As can be seen, the propylene

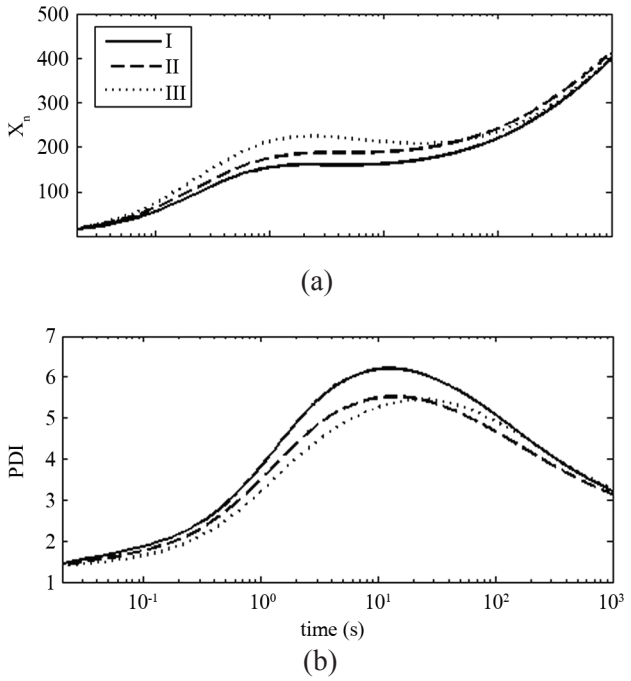

Figure 6. Dynamic evolution of the number average degree of polymerization (a) and PDI (b) for different shapes of initial catalyst (cases I, II and III).

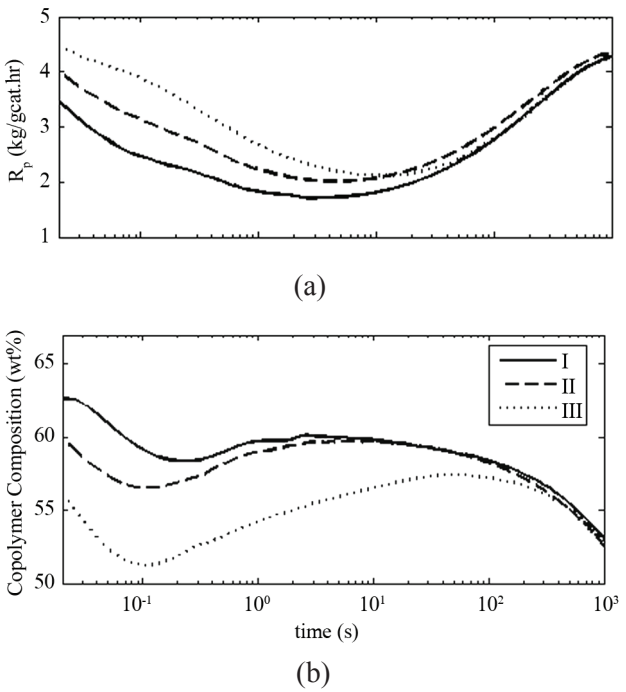

Figure 7. Dynamic evolution of the rate of polymerization (a) and propylene composition in copolymer (wt%) (b) for different shapes of initial catalyst (cases I, II and III).

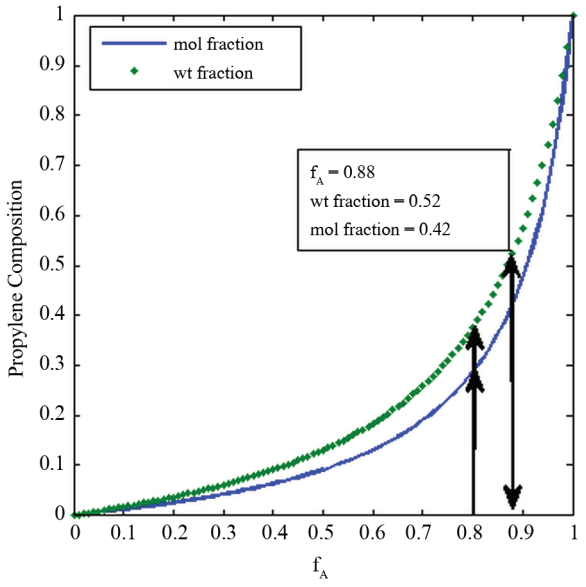

Figure 8. The molar fraction of propylene in the copolymer (F_{PA}) vs propylene molar fraction in the particle (f_A).

percent in whole particle is about 53.

If the copolymer composition is merely statistical neither affected by mass transport limitations nor the multiplicity of active site types, the molar fraction of propylene monomer in copolymer (F_{PA}) should follow from Eq. (20) [20].

$$F_{PA} = \frac{(r_A - 1) f_A^2 + f_A}{(r_A + r_B - 2) f_A^2 + 2(1 - r_B) f_A + r_B} \quad (20)$$

$$r_A = \frac{K_{pAA}}{K_{pAB}}; r_B = \frac{K_{pBB}}{K_{pBA}} \quad (21)$$

Where F_{PA} corresponds to the average propylene composition of all chains produced, r_A and r_B are the reactivity ratios and f_A is the propylene molar fraction in polymerization media. In Figure 8, F_{PA} is plotted versus f_A. As can be seen, for the values used in this simulation, the F_{PA} is about 0.28. While due to the mass transport limitation it is increased to about 0.43 (mole fraction), which is obtained when f_A is 0.884 (instead of 0.8). It should be noted that according to the kinetic constant used, the amount of reactivity ratios are the same for both sites, therefore this deviation is only caused by mass transport limitation. In conclusion, the mass transport limitations affected by the initial shape of the catalyst, caused the broad propylene composition distribution in copolymer chains. The experimental results of metallocene ethylene propylene copolymerization provided by Hoel et al. also showed a broad CCD and the mass transport limitations in polymer particles were stated as a reason [12].

Effect of crack pattern

The presented two-dimensional model makes it possible to evaluate the effect of the crack pattern on the average molecular properties. Najafi et al. [23] have studied the impact of radial and shell cracks on the reaction rate and PDI in olefin homopolymerization.

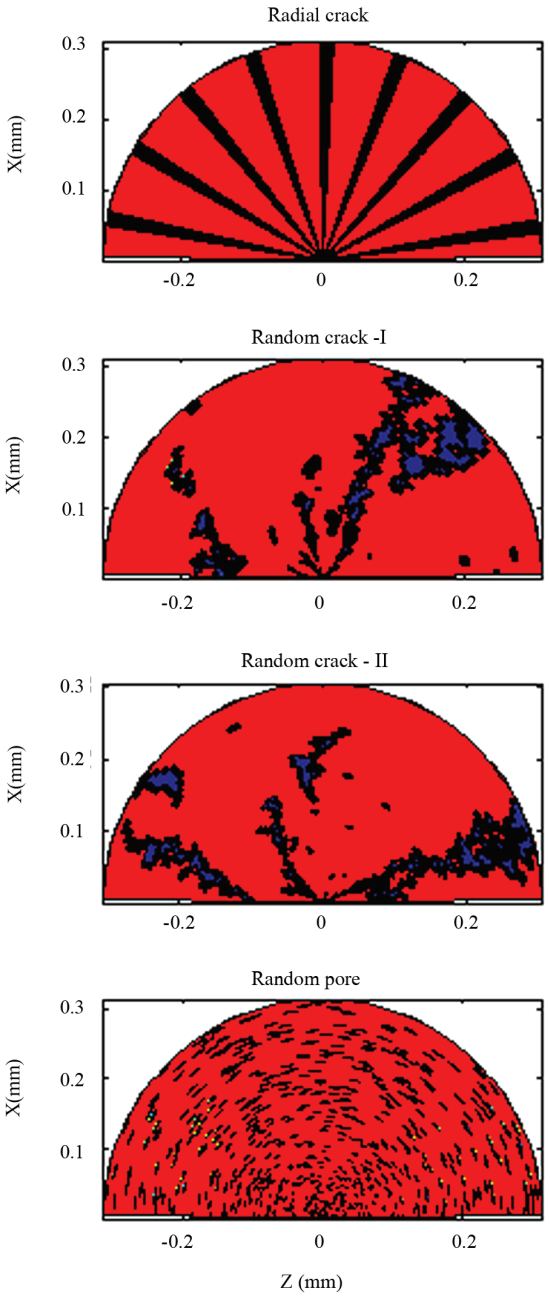

Figure 9. Different patterns of the distribution of cracks and pores in a particle (black zones indicate cracks/pores).

In this article, the effect of the random cracks consists of some randomly interconnected pores, which are closer to the SEM and TEM photographs of polymer particles cross section [25], radial crack and random pore are studied in copolymerization. Four different patterns of the distribution of cracks and pores in a particle are studied in this simulation (see Figure 9). In the case of "radial crack", the similar cracks are uniformly positioned and particle surface is attached to the center. In the "random crack I" and "random crack II" cases, the cracks made up of interconnected pores are randomly positioned and some cracks reaches to the center. "Random pore" case is an extreme case in which the completely random distributed pores are quite apart each other and no pore interconnections exist. In all cases, the volume of cracks or pores is equal to 10 percent of the whole particle volume. The diffusion coefficient of the monomers in the cracks/pores is 10 times higher than that in the compact zone of the particle.

In Figure 10, the contour plots of the rate of polymerization and propylene composition for all different crack patterns are illustrated. In the radial crack pattern, monomers access to all growing particle zones are equally increased. Hence, after a short period of time, the rate of polymerization is simply a function of radial position. On the other hand, in the two other cases where the cracks are randomly located, the effect of cracks on the polymerization rate can be clearly seen. The reaction rate in the case of random pore dependens only on the radial position which is similar to the case of no crack/pore. It is because of the difficulty of monomers to access from the surroundings media to the center. Propylene composition in growing

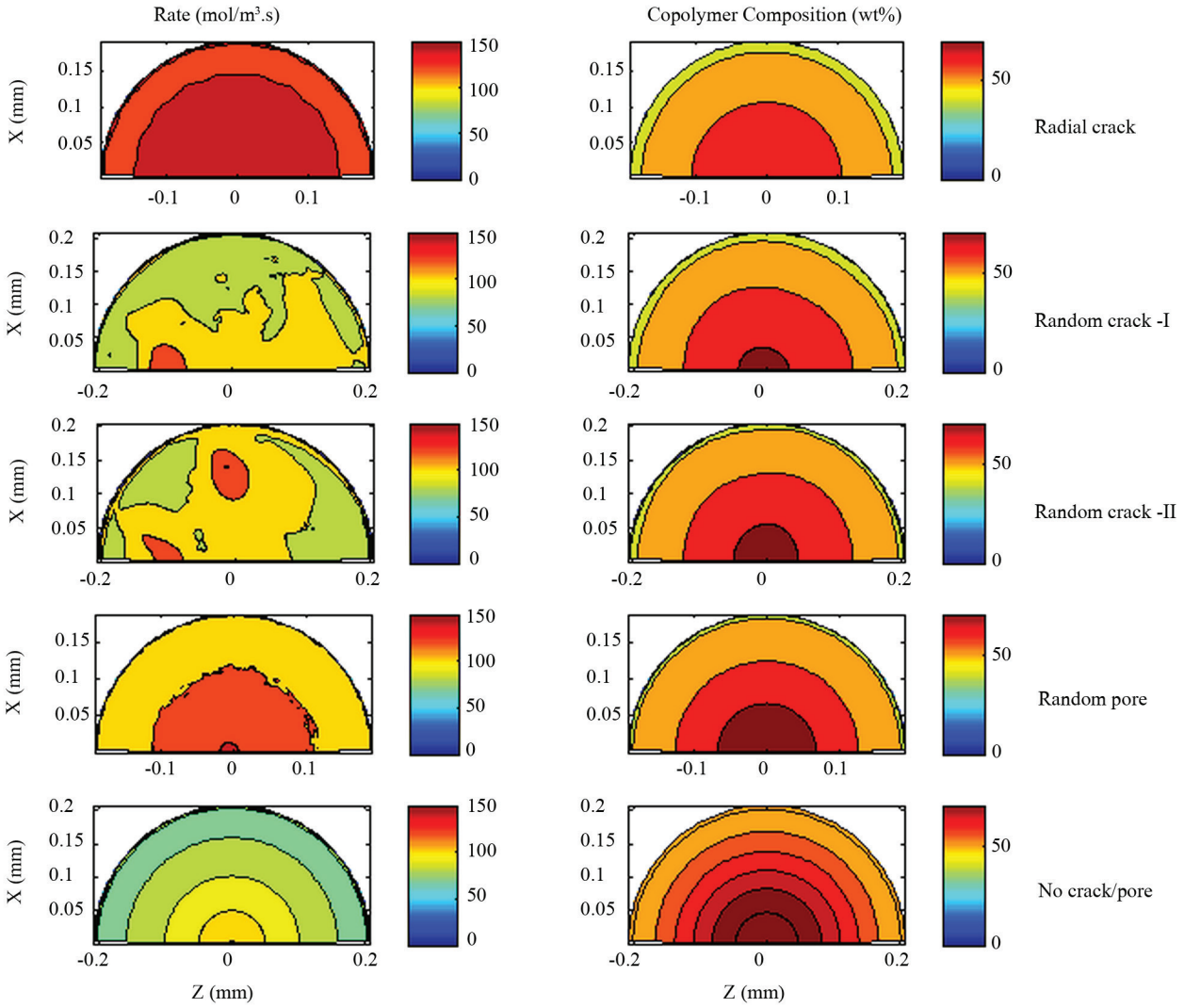

Figure 10. Contour plots of the rate of polymerization (mol/m³.s) and propylene composition in copolymer (wt%) for different crack patterns (time=300 s).

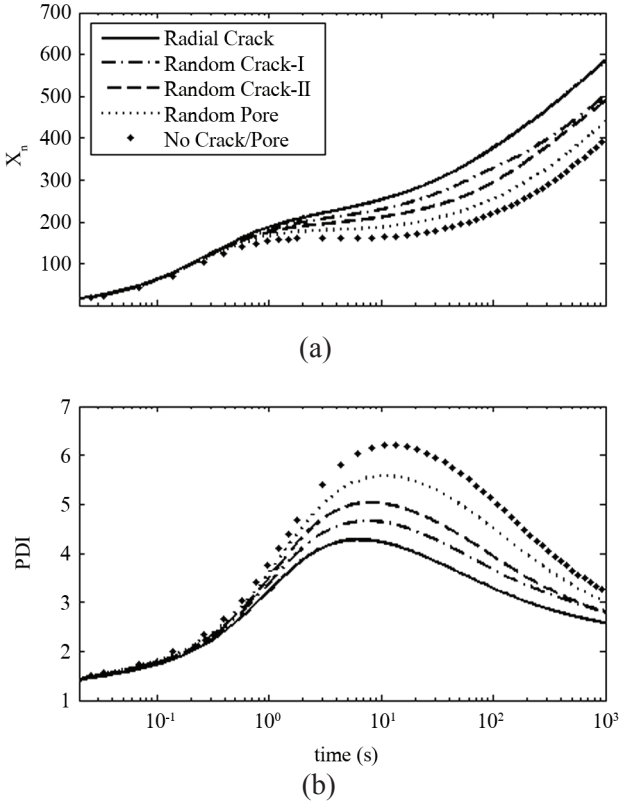

Figure 11. Dynamic evolution of the number average degree of polymerization (a) and PDI (b) for different crack patterns.

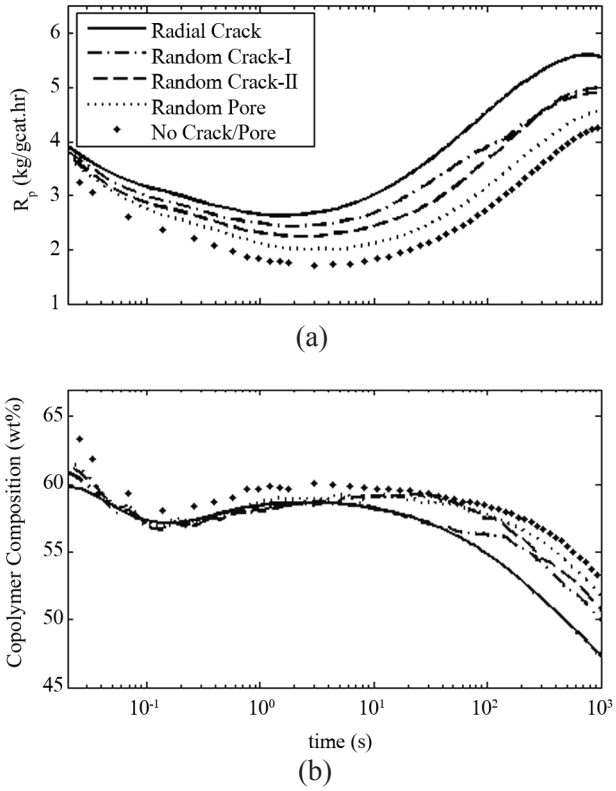

Figure 12. Dynamic evolution of the rate of polymerization (a) and propylene composition (wt%) (b) for different crack patterns.

polymer chains is also affected by the crack pattern and followed the trend of the reaction rate. In the first case, the monomer access to the particle center is easier which leads to the less propylene composition percent. In the two random crack cases, the propylene composition is almost identical and similar to the case of random pore. The polymer chains produced near the surface of the particle contain less propylene composition.

In Figure 11, the effect of crack pattern on the number average degree of polymerization ($\bar{X}_n$) and PDI are depicted. As shown in the figure, the effect of the crack pattern is decreased by increasing the polymerization time. Subsequently, the time evolution of the polymerization rate and the average propylene composition of different patterns are illustrated in Figure 12. As can be seen, the case of radial crack has the highest polymerization rate and the lowest average propylene composition because of the best monomers access to the center of the particle. To evaluate the effect of crack/pore patterns on the mass transfer limitations, the molar fraction of propylene monomer in copolymer after 1000 s is checked. As can be seen in Figure 8, for the values used in this simulation, the F_{PA} is about 0.28. While due to crack pattern it varies from 0.37 in the case of radial crack to about 0.418 in the case of random pore (mole fraction), when f_A is 0.855 or 0.878, respectively, instead of 0.8.

CONCLUSION

In the present study, a two-dimensional polymeric flow model is developed to predict the effects of the initial shape of the catalyst and crack/pore patterns on the copolymer composition, polymerization rate and average molecular weight properties for the random copolymerization of propylene-ethylene with heterogeneous Ziegler-Natta catalyst.

Three different initial shapes of catalyst from spherical to oblate ellipsoidal are considered, it is shown that the initial shape of the catalyst can change the properties in the early stage of polymerization, but after about 100 s the results are almost independent of the catalyst initial shape.

Different patterns of crack/pore inside a particle are applied to study the effect of cracks on the

molecular properties of the copolymer particle. The simulation results indicate that the crack/pore patterns in the growing particle have a strong impact on the copolymer composition in the polymer particles due to the change of mass transfer limitations.

REFERENCES

1. McKenna TF, Soares JBP (2001) Single particle modelling for olefin polymerization on supported catalysts: A review and proposals for future developments. Chem Eng Sci 56: 3931-3949
2. Dube MA, Soares JBP, Penlidis A, Hamielec, JBP (1997) Mathematical modelling of multipcomponent chain-growth polymerizations in batch, semi-batch, and continuous reactors: A review. Ind Eng Chem Res 36: 966-1015
3. Mattos Neto AG, Pinto JC (2001) Steady state modeling of slurry and bulk propylene polymerization. Chem Eng Sci 56: 4043-4057
4. Schmeal WR, Street JR (1971) Polymerization in Expanding Catalyst Particles. AIChE J 17:1188-1197
5. Singh D, Merrill RP (1971) Molecular weight distribution of polyethylene produced by Ziegler-Natta catalysts. Macromolecules 4: 599-604
6. Kanellopoulos V, Dompazis G, Gustafsson B, Kiparissides C (2004) Comprehensive analysis of single-particle growth in heterogeneous olefin polymerization: The random-pore polymeric flow model. Ind Eng Chem Res 43: 5166-5180
7. Nagel EJ, Klrillov VA, Ray WH (1980) Prediction of molecular weight distributions for high-density polyolefins. Ind Eng Chem Prod Res Dev 79: 372-379
8. Floyd S, Choi KY, Taylor TW, Ray WH (1986) Polymerization of olefins through heterogeneous catalysis. III. Polymer particle modelling with an analysis of intraparticle heat and mass transfer effects. J Appl Polym Sci 32: 2935-2960
9. Galvan R, Tirrell M (1986) Molecular weight distribution predictions for heterogeneous Ziegler-Natta polymerization using a two-site model. Chem Eng Sci 41: 2385-2393
10. Hutchinson RA, Chen CM, Ray WH (1992) Polymerization of olefins through heterogeneous catalysts X: Modelling of particle growth and morphology. J Appl Polym Sci 44: 389-1414
11. Debling JA, Ray WH (1995) Heat and mass transfer effects in multistage polymerization processes: impact polypropylene. Ind Eng Chem Res 34: 3466-3480
12. Hoel EL, Cosewith C, Byrne GD (1994) Effect of diffusion on heterogeneous ethylene propylene copolymerization. AIChE J 40: 1669-1684
13. Sarkar P, Gupta SK (1991) Modelling of propylene polymerization in an isothermal slurry reactor. Polymer 32: 2842-2852
14. Chen Y, Liu X (2005) Modeling mass transport of propylene polymerization on Ziegler-Natta catalyst. Polymer 46: 9434-9442
15. Soares JBP, Hamielec AE (1995) General dynamic mathematical modeling of heterogeneous Ziegler-Natta and metallocene catalyzed copolymerization with multiple site types and mass and heat transfer resistances. Polym React Eng 3: 61-324
16. Wang W, Zheng ZW, Luo ZH (2011) Coupled single-particle and Monte Carlo model for propylene polymerization. J Appl Polym Sci 119: 352-362
17. Najafi M, Parvazinia M, Ghoreishy MH, Kiparissides C (2014) Development of a two dimensional finite element isothermal particle model to analyse the effect of initial particle shape and breakage in Ziegler-Natta olefin polymerization. Macromol React Eng 8: 29-45
18. Soares JBP (2001) Mathematical modeling of the microstructure of polyolefins made by coordination polymerization: A review. Chem Eng Sci 56: 4131-4153
19. Ahmadi M, Nekoomanesh M, Arabi H (2010) A simplified comprehensive kinetic scheme for modeling of ethylene/1-butene copolymerization using Ziegler-Natta catalysts. Macromol React Eng 4: 135-144
20. Soares JBP, McKenna T, Cheng CP (2007) In: Polymer reaction engineering, Asua JM (ed) 1st ed, Blackwell, Ch. 2, 29-117
21. Dompazis G, Kanellopoulos V, Touloupides V, Kiparissides C (2008) Development of a multi-scale, multi-phase, multi-zone dynamic model for the prediction of particle segregation in catalytic olefin polymerization FBRs. Chem Eng Sci 63: 4735-4753
22. Soares JBP, Hamielec AE (1996) Copolymerization of olefins in a series of continuous stirred-tank slurry-reactors using heterogeneous Ziegler-Natta

and metalocene catalysts. I. General dynamic mathematical model, Polym Reac Eng 4: 153-191
23. Najafi M, Parvazinia M, Ghoreishy MH (2014) Modelling the effects of fragment patterns on molecular properties and particle overheating in olefin polymerization. Polyolefins J 1: 77-91
24. Najafi M, Parvazinia M (2015) Computational Modeling of Particle Fragmentation in the Heterogeneous Olefin Polymerization. Macromol Theory Simul 24: 28-40
25. Zubov A, Pechackova L, Seda L, Bobak M, Kosek J (2010) Transport and reaction in reconstructed porous polypropylene particle: Model validation. Chem Eng Sci 65: 2361-2372